Superfluid vortices in a wall-bounded flow

Luca Galantucci[1], Maurizio Quadrio[1], Paolo Luchini[2]
[1]*Department of Aerospace Engineering, Politecnico di Milano, Italy*
E-mail: galantucci@aero.polimi.it, maurizio.quadrio@polimi.it

[2]*Department of Mechanical Engineering, University of Salerno, Italy*
E-mail: luchini@unisa.it

Keywords: Superfluid Helium^4, wall-bounded geometries, quantized vortex-lines.

We have performed bidimensional numerical simulations of He II channel counterflows. Peculiar to this research is the presence of solid boundaries in the geometry of the system studied. The vortex-points dynamics is analyzed via a complex-potential-based algorithm which computes the temporal evolution of the vortex-points positions. The results of the research are discussed in terms of the superfluid induced velocity profile which is compared to the Poiseuille velocity profile of the normal fluid. Similarities and differences are examined and we argue that the dissimilarities between the two profiles are related to the vortex-points nucleation region and to the different dynamics that characterize vortex-points of opposite sign.

1 INTRODUCTION

The interest of the scientific community upon superfluid flows of He^4's liquid phase at temperatures T below the λ phase-transition temperature $T_\lambda = 2.17^o$K (the liquid phase is usually indicated as *He II*) significantly increased in the last ten years. This rising enthusiasm concerning superfluid physics considerably contributed in turning this branch of modern physics in one of the most important fields in low temperature physics. This increasing interest is due to three concurring motivations: i) new features recently discovered which gave birth to several new research topics regarding the peculiar characteristics of He II superflows; ii) the number of distinct physical systems where He II theoretical models can be employed; and, iii) important industrial applications of cryogenic Helium.

New insight has been also achieved thanks to the increasing computational power available to numerical simulations of the properties exhibited by the He II system. The computational cost required by a correct and accurate numerical analysis of He II superflows is ultimately related to the very wide range of spatial (and, therefore, temporal) scales which must be simultaneously resolved [1]. The most accurate and recent numerical studies of He II flows ([2, 3, 4] just to mention some of the scientific works carried out in the last ten years) would not have been able to account for the smallest dynamically significant scales and interactions without leveraging the power of modern computers. These simulations have brought to light many similarities between the so-called *Quantum Turbulence*, associated to turbulent phenomena observed in quantum liquids (i.e. fluids, as He II, where the quantum effects are predominant with respect to classical issues) and ordinary classical turbulence [5, 6, 7]. Such characteristics play a fundamental role in high-technology industrial applications of He II flows, such as cryogenic cooling systems for large-scale superconductor devices employed in high-magnitude and high-precision magnetic field generation. This technology is crucial in particle accelerators (e.g LHC at CERN, Génève, TESLA at DESY, Hamburg) and nuclear fusion experiments.

Recent large-scale simulations have also contributed to enhancing our knowledge of the dynamics of the quantized vortex-lines which are peculiar to superfluid and condensed-matter systems. The

insight gained with the numerical studies of the temporal evolution of He II quantized vortex-lines can be therefore extended to all physical systems displaying quantized vorticity and topological defects. Examples of such systems are: vortices in superconductors, internal structures of neutron stars and pulsars, dislocation in solids, disinclinations in liquid crystals, Bloch lines in magnetic materials, micro-topological defects in Bose-Einstein condensates [8].

To the best of our knowledge, however, all of the numerical studies published so far were performed in unbounded He II physical systems; in other words, none of them considered He II flows in proximity of a solid wall. The total absence of numerical simulations of He II superflows in wall-bounded geometries is one of the main motivations of the present work, that recongnizes the essential role played by solid walls in vortex-line dynamics and nucleation. Solid boundaries, in fact, strongly influence the velocity profiles of both the superfluid fraction (its wall-normal velocity component vanishes on the solid boundary) and of the normal fluid component (that is affected also by the additional no-slip condition), and therefore determine the velocity field of the quantized vortex-lines. In addition, the solid walls heavily influence the *thermally activated nucleation* of the vortex-lines by determining a particular shape of the energy barrier which must be overcome in order to produce nucleation events [9].

The numerical study presented here analyzes a bidimensional He II channel counter-flow. In the dimensionality of the problem considered the evolution of the vortex-lines is obviously replaced by the simpler *vortex-points* dynamics. The outline of the paper is as follows. After a short illustration in §2 of the peculiar characteristics of the liquid phase He II, and the numerical simulations of He II superflows performed in the past will be presented. In §3 the properties of the particular physical system considered here will be shortly described, while in §4 the characteristics of the theoretical and numerical models employed will be concisely outlined. Finally, in §5 the main results will be presented and discussed.

2 THE LIQUID PHASE He II

The intrinsic characteristics of He II have motivated several fundamental works since the first experimental results obtained employing He^4 at temperatures below T_λ. The early experiments analysing the properties of He II [10, 11] revealed the possibility of He II inviscid flows and led to the development of the *two-fluid model*. This phenomenological description of He II, elaborated separately by Landau [12, 13] and Tisza [14], considers He II as an intimate mixture of two inseparable fluid components which penetrate each other: the *normal* component and the *superfluid* component. According to this model, each fluid component has its own density and velocity fields, ρ_n and $\boldsymbol{v}_n$ for the normal fluid and ρ_s and $\boldsymbol{v}_s$ for the superfluid component. The total density of He II is $\rho = \rho_n + \rho_s$. In the two-fluid model, the viscosity and the entropy associated to the superfluid component are zero, and its flow is considered irrotational. Therefore, the superfluid component is similar to a classical, inviscid Euler fluid. The normal fluid component, on the other hand, is described as a gas of thermal excitations, named *phonons* and *rotons* according to the normal fluid linear momentum. The normal component carries the entire entropy and viscosity of He II and is therefore similar to a classical, viscous Navier-Stokes fluid.

The relative proportion of normal and superfluid components is a function of the absolute temperature T; this function has been determined experimentally by Langer & Reppy [15], Mehl & Zimmermann [16] (in liquid-helium gyroscope experiments) and Andronikashvili [17] (with the oscillating-disc experiment). The two-fluid model explains many observed characteristics of He II flows. Among them we mention the *thermal counterflow* and the *second sound propagation*. This model was found however to be incomplete. Studies by Onsager [18], London [19] and Feynman

[20], appeared in fact soon afterwards and suggested the possible existence of small regions of concentrated vorticity in the superfluid. These regions were supposed to be either bi-dimensional *vortex-sheets* [19] or one-dimensional *vortex-lines* [18, 20]. In both formulations the non-zero superfluid vorticity would be confined in the mentioned vortical structures around which the circulation of the superfluid velocity field $\boldsymbol{v}_s$ is quantized to integer multiples of h/m_4 (where h is the Planck constant and m_4 is the mass of a He^4 particle).

Soon thereafter, in 1956 Hall and Vinen [21, 22] demonstrated, both theoretically (thermodynamically) and experimentally, that the correct model for confined superfluid vorticity is the Onsager-Feynman vortex-lines formulation. In their papers, Hall and Vinen also derive a mathematical expression for the *mutual friction* force, that is the mechanism through which the two components of He II exchange momentum. Momentum transfer arises from collisions between the vortex-lines, belonging to the superfluid fraction, and the elementary excitations (phonons and rotons) which constitute the normal fluid. The mathematical expression of the mutual friction force, deduced by Hall and Vinen, and therefore valid for uniformly rotating He II only, was extended by Schwarz [23] to generic He II systems exhibiting superfluid quantized vortex-lines of any geometry. In this work, Schwarz accounts for the curvature of the vortex-lines (which is absent in uniformly rotating He II where the vortex-lines are straight) and deduces a general mathematical expression for the mutual friction force. The latter has been a crucial advancement in superfluid physics. From the general expression of the mutual friction force, in fact, Schwarz derived, in the same paper, the equation of motion of a vortex-line element, which represents the starting point and the core of the first numerical algorithms elaborated in the following decades.

Schwarz himself [24] pioneered the numerical approach, by simulating in 1988 the spatial and temporal evolution of a quantized *vortex tangle* in a thermal counterflow. Due to the computational resources available at the time, the algorithm was *kinematic*, i.e. the normal fluid and the superfluid velocities were given at the beginning of the calculations and never modified. In the following decade, the increasing computer power was leveraged by numerical codes which prescribed the motion of only one component, usually $\boldsymbol{v}_n$. Different assumptions were made about the normal fluid: uniform flow [25], Poiseuille flow [25, 26], a Gaussian vortex [27], ABC flows [28]. The kinematic approach was also used to study the behaviour of the normal fluid by assigning the topology of superfluid vortices [29].

All the different kinematic approaches listed above, however, are limited by the *a priori* prescription of at least one velocity field. The existence of the mutual friction force implies that the normal fluid velocity $\boldsymbol{v}_n$ and the superfluid vortex-lines mutually influence during their evolution. As a consequence, ten years ago Barenghi and Samuels [1] elaborated a numerical algorithm which allowed the normal fluid and the superfluid vortices to determine each other self-consistently. This computational code employs a Lagrangian algorithm, based on vortex filaments methods, to determine the spatial and temporal evolution of the discrete vortex-lines elements and an Eulerian calculation, based on modified Navier-Stokes equations, to resolve the normal fluid velocity field. The algorithm employed by Barenghi and Samuels was later slightly modified by Idowu *et al.* [2] to take into account the extreme locality of the mutual friction force in the circumstance of a quantized vortex tangle numerical simulation.

3 THERMAL COUNTERFLOW

The thermal counterflow, that is the subject of this paper, is a unique fluid dynamic phenomenon existing in He II. It is a direct consequence of the two-fluid structure which characterizes the liquid phase. As the dominant heat transfer process in He II, thermal counterflow has been extensively

analyzed since its discovery in 1950s, focusing especially on two major aspects: i) the hydrodynamic characteristics of the two fluid components and their interaction under different physical conditions; ii) the fundamentals of vortex-lines dynamics and their effects on the hydrodynamics of the two fluid components. A typical experimental setup [30, 31] is illustrated in Fig. 1. Two He II reservoirs

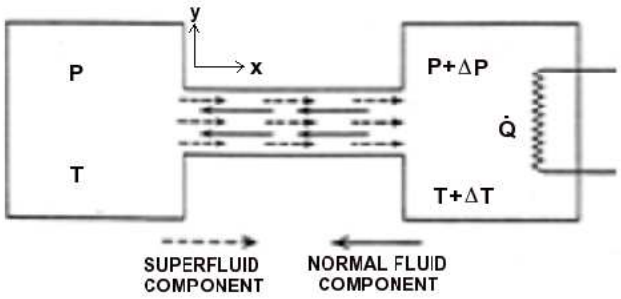

Figure 1: He II thermal counterflow experimental setup

are connected by a channel whose width 2δ is small with respect to its length L_x and depth L_z. A heater placed in one of the reservoirs supplies a constant heat flux and creates a uniform temperature gradient ∇T across the channel. Since entropy is only carried by the normal fluid, the heat transfer by the normal flow is the only mechanism of heat transfer in He II which is, therefore, of the nature of convection [32]. As a consequence, the heat density flux vector $\boldsymbol{q}$ in the channel is given by the following identity

$$\boldsymbol{q} = \rho s T \overline{\boldsymbol{v}}_n \tag{1}$$

where s is the entropy per unit mass and $\overline{\boldsymbol{v}}_n$ is the normal fluid velocity averaged over a channel cross section. Mass conservation implies a zero net mass flux over the channel cross sections and allows the calculation of the uniform velocity field of the superfluid fraction which, added to the vortex-lines'induced velocity, constitutes $\boldsymbol{v}_s$.

The He II thermal counterflow, as anticipated, can be easily understood in terms of the two-fluid model. According to the latter, the equations of motion of the two fluid components are the following:

$$\rho_n \frac{\partial \boldsymbol{v}_n}{\partial t} + \rho_n \left(\boldsymbol{v}_n \cdot \nabla\right) \boldsymbol{v}_n = \eta_n \nabla^2 \boldsymbol{v}_n - \frac{\rho_n}{\rho} \nabla p - \rho_s s \nabla T \tag{2}$$

$$\rho_s \frac{\partial \boldsymbol{v}_s}{\partial t} + \rho_s \left(\boldsymbol{v}_s \cdot \nabla\right) \boldsymbol{v}_s = \frac{\rho_s}{\rho} \nabla p + \rho_s s \nabla T \tag{3}$$

where η_n is the dynamic viscosity coefficient of the normal fluid. If there is no explicit time dependence of the velocity fields and the latter are either very small or laminar, the equations (2) and (3) reduce to London's equation

$$\nabla p = \rho s \nabla T \tag{4}$$

and Poiseuille's equation for classical hydrodynamics

$$\nabla p = \eta_n \nabla^2 \boldsymbol{v}_n \tag{5}$$

Equation (4) is very important because it states that a temperature gradient implies the simultaneous presence of a pressure gradient. The latter causes the flow of the normal fluid which is characterized by a parabolic velocity profile obtained by the integration of equation (5) with the standard no-slip boundary conditions. The normal fluid velocity profile is given by the following expression

$$\boldsymbol{v}_n(\boldsymbol{x}) = -v_n(y)\hat{\boldsymbol{x}} = \frac{|\nabla p|}{2\eta_n} y(y-2\delta)\hat{\boldsymbol{x}} \tag{6}$$

where $v_n(y) \geq 0$. The uniform superfluid velocity field is obviously directed in the opposite direction in order to satisfy mass conservation. Under the current hypotheses, temperature and pressure gradients are a linear function of the steady heat flux $\dot{Q}$ supplied by the heater [30].

The condition of time-independent and small velocity fields is valid as long as $\dot{Q}$ is smaller than a threshold value. Above this threshold, the dynamics of the two He II fluid components undergo a change, due to the nucleation of vortex-lines which interact with both the normal and the superfluid fractions. This interaction, at constant heat flux $\dot{Q} > \dot{Q}_*$, is responsible for an increase of the magnitude of the temperature and pressure gradients.

4 THE MODEL

The algorithm elaborated in the present work performs the two dimensional numerical simulation of the dynamics of N vortex-points. The latter are the intersections of N straight vortex-lines with the channel's longitudinal cross section which coincides with our computational domain. The bidimensionality of the system implies that all the N vortex-lines are parallel to the z axis which is orthogonal to the channel's section considered. The mathematical expression employed for the velocity $\boldsymbol{v}_L$ of a generic vortex-point is the bidimensional version of the expression deduced by Schwarz in [23]:

$$\boldsymbol{v}_L = \boldsymbol{v}_s^{ext} + \boldsymbol{v}_{s,i} + \alpha \boldsymbol{s}' \times \left(\boldsymbol{v}_n - \boldsymbol{v}_s^{ext} - \boldsymbol{v}_{s,i}\right) + \alpha' \left(\boldsymbol{v}_n - \boldsymbol{v}_s^{ext} - \boldsymbol{v}_{s,i}\right) \tag{7}$$

In the expression above, α and α' are temperature-dependent adimensional friction coefficients related to Hall and Vinen's [21, 22] constants B and B' by the expressions $\alpha = \dfrac{\rho_n B}{2\rho}$, $\alpha' = \dfrac{\rho_n B'}{2\rho}$; $\boldsymbol{v}_{s,i}(\boldsymbol{x}, t)$ is the superfluid induced velocity field generated by the remaining $N-1$ vortex-points; $\boldsymbol{v}_s^{ext} = v_s^{ext}\hat{\boldsymbol{x}}$ is the uniform superfluid velocity field which is characteristic of thermal counterflows and guarantees a zero net mass flow across the channel; $\boldsymbol{s}'$ is the unit vector tangent to the vortex-line ($\boldsymbol{s}' = \pm\hat{\boldsymbol{z}}$ depending on the sign of the vortex-point); $\boldsymbol{v}_n(\boldsymbol{x})$ is the velocity field of the normal fluid which is still given by expression (6). In fact, for simplicity, in the present work the feedback of the vortex-lines'motion on the normal fluid is neglected and, therefore, the Poiseuille profile (6) is valid provided that ∇p is replaced by ∇p_{tot}, in order to considerthe effect of the vortex-lines on the pressure field.

In the geometry analyzed in this study and with axes oriented as shown in Fig. 1, the expression (7) for the velocity of the k-th vortex-point, whose position at a generic instant t is $(x_k(t), y_k(t))$, assumes the following form:

$$\begin{aligned} \boldsymbol{v}_L(x_k, y_k, t) \quad = \quad & \left[(1-\alpha')\left(v_s^{ext} + v_{s,i}^x\right) - \alpha' v_n(y) \pm \alpha v_{s,i}^y\right]\hat{\boldsymbol{x}} + \\ & + \left[(1-\alpha')\, v_{s,i}^y \mp \alpha\left(v_n(y) + v_s^{ext} + v_{s,i}^x\right)\right]\hat{\boldsymbol{y}} \end{aligned} \tag{8}$$

The reasons why in the realization of the algorithm we employ Schwarz's formulation instead of Idowu *et. al*'s [2], which accounts for the locality of the mutual friction force, are three: (a) in the

present work, as affirmed previously, we have not considered the feedback of the vortex-lines on the normal fluid velocity field; (b) the absence of the vortex-lines' auto-induction velocity field and (c) the constant direction of $\boldsymbol{s}'$ due to the fact that the vortex-lines, in the bidimensional geometry considered in this work, do not present any curvature.

The superfluid induced velocity field $\boldsymbol{v}_{s,i}$ generated by the remaining $N-1$ vortex-points is computed employing a complex-potential-based formulation. The latter is applicable in the system studied due to bidimensionality of the flow, the irrotationality of the velocity field created by each single vortex-point (the vorticity field is the sum of N Dirac δ-functions centered in the vortex-points) and the incompressibility of the flow. The latter property of the flow is valid even if a temperature gradient is present across the channel. In counterflow experiments, in fact, the order of magnitude of the temperature difference is $10^{-3\circ}$K. This temperature gap between the two He II reservoirs is not sufficient to create an appreciable variation of the normal and superfluid densities $\rho_n(T)$ and $\rho_s(T)$.

The mathematical expressions of the complex potential of the flow and the corresponding complex velocity is deducible employing two equivalent but different methods. The first of the latter is based on the properties of *conformal mappings* [33, 34]. With the means of these transformations it is in fact possible to determine the mathematical expression of the complex potential of a single vortex-point in a channel by mapping conformally the latter in the upper imaginary half-plane. In this transformed geometry the expression of the complex potential $w_j(z)$ is easily determinable due to the fact that only one vortex-point image must be considered. The result obtained in the mapped geometry is then re-transformed in the original geometry employing the inverse conformal map.

The second theoretical framework which is possible to employ in order to derive the expression of the complex potential considers, instead, the infinite pair of images of a single vortex-point and its complex conjugate with respect to the channel's walls [35]. The complex potential of a vortex-point is then obtained computing the series which originates from summing the infinite complex potentials of the vortex- point, its complex conjugate and the corresponding images. This last method coincides with the framework employed in the present work in which, for brevity, we will only report the results of the theoretical study realized by Greengard [35].

The complex potential $w_j(z)$ of the j-th vortex-point z_j in a channel flow is given by the following expression

$$w_j(z) = \mp\imath\frac{h}{2\pi m}\log\frac{\sinh\left[\frac{\pi}{4\delta}\left(z-z_j\right)\right]}{\sinh\left[\frac{\pi}{4\delta}\left(z-\overline{z_j}\right)\right]} \tag{9}$$

where $\dfrac{h}{m}$ is the quantum of circulation (h is Planck's constant) and the $\mp$ in front of the right hand side of (9) depends on the sign of vortex-point. The consequent complex velocity field $v_j(z)$ is then given by the following identity

$$v_j(z) = v_j^x - \imath v_j^y = \mp\imath\frac{\hbar}{m}\frac{\pi}{4\delta}\left\{\coth\left[\frac{\pi}{4\delta}\left(z-z_j\right)\right] - \coth\left[\frac{\pi}{4\delta}\left(z-\overline{z_j}\right)\right]\right\} \tag{10}$$

where $\hbar = \dfrac{h}{2\pi}$. The complex superfluid induced velocity field $v_{s,i}(z_k)$ in the position occupied by the k-th vortex point is finally given by the following expression

$$v_{s,i}(z_k) = v_{s,i}^x - \imath v_{s,i}^y = \sum_{j\neq k} v_j(z_k) \pm \imath\frac{\hbar}{m}\frac{\pi}{4\delta}\coth\left[\frac{\pi}{4\delta}\left(z_k-\overline{z_k}\right)\right] \tag{11}$$

where $z_k = x_k + \imath y_k$ and the last term is the complex velocity generated by its complex conjugate $\overline{z_k}$.

$T(^\circ K)$	ρ_n/ρ_s	α	α'	$\Delta p_{tot}(Pa)$	$L_x(m)$	$\eta_n(Pa\cdot s)$	$\delta(m)$
1.5	0.143	0.078	6.25×10^{-3}	10	0.1	3×10^{-7}	3×10^{-5}

Table 1: Numerical values of the relevant physical quantities characterizing the thermal counterflow analyzed in this work

The periodicity in the x direction is treated only partially, i.e. we have considered only one vortex-point image with respect to the computational domain's boundaries in the x direction. Employing this procedure an error decreasing exponentially with the aspect ratio of the channel is committed and, therefore, to minimize this error it is sufficient to consider a channel whose length is significantly larger than its width.

The velocity field $\boldsymbol{v}_s^{ext}$ is instead determined imposing a zero net mass flux condition in the x direction

$$\boldsymbol{v}_s^{ext} = -\frac{\rho_n}{\rho_s}\overline{\boldsymbol{v}}_n \tag{12}$$

(the superfluid mass flux arising from the velocity field $\boldsymbol{v}_{s,i}$ is neglected in the present work). Having determined all the terms which appear in equation (8) the numerical code elaborated in the present work computes the temporal evolution of the positions of the N vortex-points starting from completely random N initial positions. In the circumstance where a vortex-point collapses on a wall the number of vortex-points is kept constant by nucleating a vortex-point in a position where its velocity is zero due to the simultaneous action of $\boldsymbol{v}_s^{ext}$ and the velocity field generated by its complex conjugate. This distance from the walls (positive vortex-points will nucleate close to the upper wall while the negative ones in proximity of the lower) is indicated with y^* and it is given by the following expression:

$$y^* = \frac{2}{\pi}\arctan\left(\frac{\pi}{4}\frac{1}{v_s^{ext}}\right) \tag{13}$$

5 NUMERICAL RESULTS AND DISCUSSION

The values of the relevant physical quantities characterizing the system studied in this work are extracted by the experimental data illustrated by Childers & Tough in [30] and are reported in Table 1. The values of Δp_{tot} and L_x employed generate a total pressure gradient $\nabla p_{tot} = 100 Pa/m$. The latter, with the values of η_n and δ reported in Table 1, implies that $\overline{v}_n = 0.10 m/s$ and $v_s^{ext} = 0.014 m/s$.

Employing these numerical values we have realized numerical simulations of a He II thermal channel counterflow. We have focused the attention on the superfluid induced velocity profile $\langle v_{s,i}^x \rangle(y)$. The $\langle\cdot\rangle$ operator denotes an average taken over the x direction (analitical average) and over time (numerical average). The results obtained can be observed in Fig. 2 where two velocity profiles corresponding to two different values of the vortex-points number N are plotted.

The first observation which can be made is that the velocity profiles tend to assume an almost parabolic profile, i.e. a profile which is qualitatively similar to the normal fluid velocity profile. This qualitative locking between $\boldsymbol{v}_{s,i}$ and $\boldsymbol{v}_n$ has already been observed by Samuels in laminar pipe flow of He II [26] and Barenghi *et al.* in regions of high magnitude normal fluid vorticity [28].

The reason why the superfluid induced velocity profile $\langle v_{s,i}^x \rangle(y)$ has the nearly parabolic y dependence shown in Fig. 2 is the different dynamics to whom positive and negative vortex-points are subject. From equation (8), in fact, it can be easily observed that the y component of $\boldsymbol{v}_L$ has an opposite sign for positive and negative vortex-points. More precisely, positive vortex-points have a

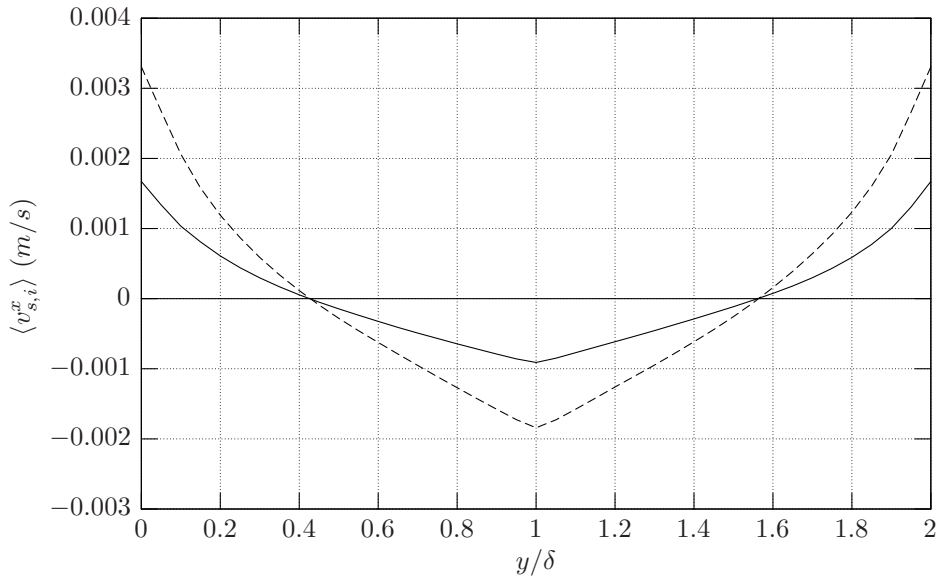

Figure 2: Superfluid induced velocity profile $\langle v^x_{s,i} \rangle$ for $N = 10$ (continuous line) and $N = 20$ (dashed line)

negative v^y_L and move therefore towards the bottom wall, while the negative vortex-points migrate towards the top wall. As a consequence, a vortex-point *sign-separation* takes place and produces the superfluid induced velocity profile illustrated in Fig. 2.

However, despite the similarities between the shape $\langle v^x_{s,i} \rangle(y)$ and $v_n(y)$, two main differences can be observed in Fig. 2. The first dissimilarity between the two profiles can be noticed in the central region of the channel where the superfluid induced velocity profile shows a peak. This is due to the fact that in our numerical simulations $y^* \sim \delta$ and therefore both positive and negative vortex-points nucleate in proximity of the channel's centerline. Immediately after their respective nucleation, the vortex-points move towards the walls as explained in the previous paragraph generating a relatively large negative value of $v^x_{s,i}$ in the central region of the channel. This phenomenon, which concerns all the nucleated vortex-points, accounts for the peaked shape of $\langle v^x_{s,i} \rangle(y)$ near the channel's centerline. The second qualitative difference between $\langle v^x_{s,i} \rangle(y)$ and $v_n(y)$ regards the behaviour in the near-wall region. In the latter, in fact, $\langle v^x_{s,i} \rangle(y)$ is positive due to the combined action of the vortex-points and their nearest images with respect to the wall. The plots of $\langle v^x_{s,i} \rangle(y)$ reported in Fig. 2 also show, as it could have been expected, that a larger value of N implies to larger absolute values of $\langle v^x_{s,i} \rangle(y)$.

The values of $\langle v^x_{s,i} \rangle(y)$ reported in Fig. 2 imply that the superfluid mass flux which originates from the induced field $\boldsymbol{v}_{s,i}$ must be considered while computing the total superfluid mass flux. As a consequence, the expression (12) for $\boldsymbol{v}_s^{ext}$ is no longer valid and should be replaced by a time-dependent expression which takes into account the superfluid mass flux arising from $\boldsymbol{v}_{s,i}$. This issue and the feedback of the motion of the vortex-lines on the normal fluid velocity field are relevant topics which will be treated in future works.

References

[1] Barenghi, C. and Samuels, D. (1999) Self-consistent decay of superfluid turbulence. *Phys. Rev. B*, **60**, 1252.

[2] Idowu, O., Kivotides, D., Barenghi, C., and Samuels, D. (2001) Numerical methods for coupled normal-fluid and superfluid flows in helium ii. *Lecture Notes in Physics*, **571**, 162.

[3] Kivotides, D. (2007) Relaxation of superfluid vortex bundles via energy transfer to the normal fluid. *Phys. Rev. B*, **76**, 054503.

[4] Hanninen, R., Tsubota, M., and Vinen, W. (2007) Generation of turbulence by oscillating structures in superfluid helium at very low temperatures. *Phys. Rev. B*, **75**, 064502.

[5] Walmsley P.M. and Golov A. I. (2008) Quantum and quasi-classical types of superfluid turbulence. *Phys. Rev. Lett.*, **100**, 245301.

[6] Tsubota M. (2008) Quantum Turbulence. *Journal of the Physical Society of Japan*, **77**, 111006.

[7] Vinen W. F. and Niemela J. J. (2002) Quantum Turbulence. *J. Low Temp. Phys.*, **128**, 167.

[8] Sonin, E. B. (1987) Vortex oscillations and hydrodynamics of rotating superfluids. *Rev. Mod. Phys.*, **59**, 87.

[9] Donnelly, R. J. and Roberts, P. H. (1971) Stochastic theory of the nucleation of quantized vortices in superfluid helium. *Phil. Trans. R. Soc. London Ser. A*, **271**, 41.

[10] Kapitza, P. (1938) Viscosity of liquid helium below the λ point. *Nature*, **141**, 74.

[11] Allen, J. F. and Misener, A. D. (1938) Flow of liquid helium ii. *Nature*, **141**, 75.

[12] Landau, L. (1941) *J. Phys. U.S.S.R.*, **5**, 71.

[13] Landau, L. (1947) *J. Phys. U.S.S.R.*, **11**, 91.

[14] Tisza, L. (1947) The theory of liquid helium. *Phys. Rev.*, **72**, 838.

[15] Langer, J. S. and Reppy, J. D. (1970) *Progress in Low Temperature Physics*, vol. VI. North Holland Publishing Co.

[16] Mehl, J. B. and Zimmermann, W. (1968) Flow of superfluid helium in a porous medium. *Phys. Rev.*, **167**, 214.

[17] Andronikashvili, E. L. (1946) *J. Phys. U.S.S.R.*, **10**, 21.

[18] Onsager, L. (1949) Statistical hydrodynamics. *Nuovo Cim.*, **6**, 249.

[19] London, F. (1954) *Superfluids*, vol. 2. Wiley, New York.

[20] Feynmann, R. (1955) *Application of quantum mechanics to liquid helium*, vol. 1, chap. II, p. 36. North Holland Publishing Co.

[21] Hall, H. and Vinen, W. (1956) The rotation of liquid helium ii. i. experiments on the propagation of secound sound in uniformly rotating helium ii. *Proc. R. Soc. London A*, **238**, 204.

[22] Hall, H. and Vinen, W. (1956) The rotation of liquid helium ii. ii. the theory of mutual friction in uniformly rotating helium ii. *Proc. R. Soc. London A*, **238**, 215.

[23] Schwarz, K. (1978) Turbulence in superfluid helium: steady homogenous counterflow. *Phys. Rev. B*, **18**, 245.

[24] Schwarz, K. (1988) Three-dimensional vortex dynamics in superfluid he4. *Phys. Rev. B*, **38**, 2398.

[25] Aarts, R. G. K. M. and de Waele, A. T. A. M. (1994) Numerical investigation of the flow properties of he ii. *Phys. Rev. B*, **50**, 10069.

[26] Samuels, D. (1992) Velocity matching and poiseuille pipe flow of superfluid helium. *Phys. Rev. B*, **46**, 11714.

[27] Samuels, D. (1993) Response of superfluid vortex filaments to concentrated normal-fluid vorticity. *Phys. Rev. B*, **47**, 1107.

[28] Barenghi, C., Samuels, D., Bauer, G., and Donnelly, R. J. (1997) Superfluid vortex lines in a model turbulent flow. *Phys. Fluids*, **9**, 2631.

[29] Barenghi, C. and Melotte, D. (1998) Transition to normal fluid turbulencein helium ii. *Phys. Rev. Lett.*, **80**, 4181.

[30] Childers, R. K. and Tough, J. T. (1976) Helium ii thermal counterflow: Temperature- and pressure-difference data and analysis in terms of the vinen theory. *Phys. Rev. B*, **13**, 1040.

[31] Henberger, J. D. and Tough, J. T. (1982) Uniformity of the temperature gradient in thr turbulent counterflow of he ii. *Phys. Rev. B*, **25**, 3123.

[32] Landau, L. and Lifshitz, E. (1959) *Fluid Mechanics*, *Course of Theoretical Physics*, *Volume 6*. Pergamon, London.

[33] Saffman, P. G. (1992) *Vortex dynamics*. Cambridge University Press.

[34] Batchelor, G. K. (1967) *An Introduction to Fluid Dynamics*. Cambridge University Press.

[35] Greengard, L. (1990) Potential flow in channels. *SIAM J. Sci. Stat. Comput.*, **11**, 603.